RSC Advances

ROYAL SOCIETY OF CHEMISTRY

www.rsc.org/advances

Journal Name

ARTICLE

Carbon dots grafted $SrAl_2O_4$:Eu,Dy dual-emitting phosphor for ratiometric temperature sensing

Received 00th January 20xx,
Accepted 00th January 20xx

DOI: 10.1039/x0xx00000x

www.rsc.org/

Bingfu Lei,[a] Wei Li,[a] Haoran Zhang,[a] Jin Wang,[a] Yingliang Liu,*[a] Jianle Zhuang[a] and Shi Chen*[a]

A simple and effective strategy has been carried out for designing ratiometric temperature sensor in this work. The carbon dots (CDs), which benefit from surface methoxysilyl groups after using an organosilane as a coordinating solvent, are highly reactive intermediates responsible for bonding with silanols and hydroxyl groups from the silica-coated $SrAl_2O_4$:Eu,Dy phosphor (SAO). Hence, the CDs grafted $SrAl_2O_4$:Eu,Dy phosphor (CDs-SAO) could be realized by a facile one-step sol-gel method. The as-prepared CDs-SAO shows characteristic fluorescence emissions of CDs (blue) and SAO (green) under a single wavelength excitation. The temperature dependence of the fluorescence intensity ratios for the two emission bands was studied, and it turned out that the composite has a wide linear temperature sensing range, which matches well with the physiologically relevant temperatures. This rather simple approach for creating dual emissions enables a completely new strategy for application of these composite in temperature sensing.

1 Introduction

Temperature is a significant physiological property that affects the chemical and biological processes. Conventional temperature sensors are obtained by heat flow to an invasive probe, the so-called contact thermometers could not remotely reporting local temperature with high spatial resolution, for instance, within individual cells of a complex cellular condition. Recently, in terms of temperature sensing, fluorescence-based measurements such as those on the basis of rare-earth ions activated luminescent materials,[1-2] semiconductor nanocrystals,[3-5] polymers,[6-7] have attracted much attention. Fluorescence-based temperature sensing is outstanding due to the merits of being noninvasive and robust in even strong electromagnetic fields. Most optical methods for measuring temperature can be divided into two categories.[8-9] The first category of temperature sensing is based on the temperature dependence of the absorption of certain materials, including thermochromic, gas band edge absorptions that shift with temperature and so on. The second type relies on luminescence temperature dependence, such as the changes in energy, intensity or decay lifetime. As measuring the luminescence lifetime requires a relatively long time and post-processing computational treatment, the intensity-based approach is more applicable for real-time temperature sensing.[10]

Fluorescent carbon dots (CDs), which consist a fascinating class of fluorescence-based nanoparticles, have drawn increasing attention because of their attractive applications in biomedical imaging.[11-12] They show strong absorption in the near UV spectral region and the efficient blue light emission which up to 80% quantum yield (QY) for solution-based particles.[13] Recent exciting progresses on CD-based optoelectronic and energy devices, such as light emitting diodes (LEDs), solar cells (SCs), photocatalysis, batteries, and supercapacitors have drawn extensive attention.[14] In this work, we have found that the CDs possess temperature-sensitive photoluminescence (PL) properties. Noninvasive optical methods are useful for determining temperatures in small confined spaces.[15] Although QDs,[16] organic dyes,[17] and polymers[6-7] have been applied as temperature sensors previously, their cytotoxicity, poor photostability, and tedious probe preparation procedures are problematic.[15]

To apply the excellent biocompatibility, eco-friendly CDs in practical device applications, it is of great importance to embed them in a proper solid matrix or prepare in solid-state architectures. Zeng's group selected poly vinyl alcohol (PVA) as a precursor to synthesize intercrossed carbon nanorings, which enable them to overcome the aggregation induced quenching effect,[18] while Shen's group integrated water soluble CDs with starch.[19] Organically modified silicates and silica gel are superior owing to their inherent stability and nontoxicity among the possible matrices, which would allow direct incorporation into existing lighting formats.[20-22] Recently, the appropriateness of rare earth doped materials for temperature sensing purpose is dominant because of the presence of large number of thermally coupled levels and high transition probabilities of nonradiative relaxations.[23-24] The erbium,

[a] *Guangdong Provincial Engineering Technology Research Center for Optical Agriculture, College of Materials and Energy, South China Agricultural University, Guangzhou 510642, China. E-mail:* ***tliuyl@163.com (Y. Liu)****,* ***kkt@scau.edu.cn (S.Chen)****. Tel. : +86-20-85280323; Fax. : +86-20-85285026*

europium, holmium, thulium, samarium, dysprosium, neodymium, praseodymium and ytterbium ions have been assigned mainly as dopants for temperature sensing applications due to availability of numerous thermally coupled levels.[25-26] $SrAl_2O_4$:Eu,Dy is advantageous due to its high brightness, enhanced chemical and thermal stabilities. Herein, CDs grafted $SrAl_2O_4$:Eu,Dy phosphor could be realized by a facile one-step sol-gel method through the hydrolysis of tetraethyl orthosilicate (TEOS).

We, for the first time, incorporated CDs with $SrAl_2O_4$:Eu,Dy phosphor (SAO), and made use of the dual-emitting from CDs and SAO within such a composite to realize ratiometric temperature sensing in physiological temperature range. Because SAO emission is highly temperature dependent while the CDs emission is less sensitive to temperature, we used CDs emission as an internal reference to construct a ratiometric temperature sensor. Compare to single intensity-based measurements, fluorescence ratiometric methods are more robust and convenient in actual applications, due to the built-in calibrations provided by simultaneous detection of two signals under one single wavelength excitation, overcoming the inaccuracy of the probe concentration and of the drifts of the optoelectronic system such as lamps and detectors.

2 Experimental

2.1 Materials and reagents

$SrCO_3$ (AR), $Al(OH)_3$ (AR), Eu_2O_3 (99.99%), and Dy_2O_3 (99.99%) were purchased from Aladdin Industrial Co., Shanghai, China. Tetraethyl orthosilicate (TEOS) was purchased from Kermel Chemical Co., Tianjing, China. Anhydrous citric was purchased from Aladdin Industrial Co., Shanghai, China. N-(β-aminoethyl)-γ-aminopropyl methyldimethoxy silane (AEAPMS) was purchased from Shenda Fine Chemical Co., Ltd, Beijing, China. Ethanol (AR) was supplied by Guanghua Co., Ltd, Guangdong, China. Hydrochloric acid (AR) was purchased from Hengyang Chemical Co., Hunan, China. All the initial chemicals in this work were used without further purification and deionized water was used throughout this work.

2.2 Synthesis of SAO

According to the literature,[27] $SrAl_2O_4$:1%Eu^{2+}, 2%Dy^{3+} phosphor was synthesized by appropriate amounts of starting materials including $SrCO_3$, $Al(OH)_3$, Eu_2O_3, and Dy_2O_3 were together ground in a ball mill for 2 h. The mixture was pressed into pellets and calcined at 1300 °C in a reducing atmosphere of flowing 3%H_2-97%N_2 for 3 h. And the fired pellets were pulverized and ground into powders.

2.3 Synthesis of CDs

CDs were synthesized according to a reported method.[12] Briefly, 10 ml AEAPMS was placed into a 100 ml three-necked flask, and degassed with nitrogen for 15 min. Heat was applied, until the temperature reached 240°C, 0.4 g anhydrous citric acid was added quickly under vigorous stirring. After 5 min, the reaction stopped and cooled to room temperature. Then the product was purified by precipitation with petroleum ether three times. A volume of 1 mL of final product was taken into 1 mL ethanol and adjusted the pH to 6.5 by addition of hydrochloric acid.

2.4 Initial sols preparation

The initial sols were prepared in two steps. First, a prehydrolysed sol (TEOS:ETOH:HCl:H_2O = 1 : 4 : 0.1 : 0.8 in molar ratio) was prepared by refluxing for 90 min. After cooling of the solution to room temperature, certain amount of H_2O and HCl was added to the solution for another 15 min stirring. The final molar ratio of constituents was TEO:ETOH: HCl:H_2O = 1 : 4 : 0.2 : 5.

2.5 Preparation of CDs-SAO

For preparation of CDs-SAO, 1g CDs solution was added into 10.0 mL initial sols under magnetic stirring, and then SAO (the mass ratio of SAO to CDs solution: 0, 0.4, 0.8, 1.2, 1.6, 2.0) was added afterward, kept stirring until a uniform gel formed under room temperature. The derived gel was dried under vacuum at 80 °C for 12 h, then grinded the xerogel into powders as the final CDs-SAO.

2.6 Characterizations

X-ray photoelectron spectroscopy (XPS) was detected by employing an X-ray photoelectron spectroscope (AXIS ULTRA DLD, Kratos). The FT-IR spectra were taken on a Nicolet Avatar 360 Fourier transformation infrared spectrophotometer. Transmission electron microscopy (TEM) images were recorded with a FEI Tecnai 12 transmission electron microscope and the high resolution transmission electron microscopy (HRTEM) images were recorded by a JEOL-2010 electron microscope. The UV-Vis absorption was recorded by a ultraviolet-visible spectrofluorometer (UV-2550, Shimadzu). Photoluminescence spectra were recorded with a fluorescence spectrofluorometer (F-7000, Hitachi). The temperature-dependent photoluminescence emission spectra were conducted by a heating apparatus (OXFORD Instrument) in combination with the same Hitachi F-7000 fluorescence spectrophotometer. The decay lifetimes were recorded on a spectrofluorometer (HORIBA, JOBIN YVON FL3-21).

3 Results and Discussion

CDs-SAO was prepared via a facile one-step sol-gel method, involved the processes of hydrolysis and polycondensation of a sol-gel precursor (TEOS). As illustrated in **Fig. 1**, the produced hydration silicon dioxide or low polymeric hydration silicon dioxide will adsorb -OH on the phosphor surface and start precipitating to form precipitation nuclei, the following SiO_2 will further precipitate on these nuclei so that a silica layer will continuously form.[28] During the processes of hydrolysis and polycondensation of TEOS, CDs could couple on the silica layer through the silylation reaction at the same time. The CDs used herein, were synthesized on the basis of the reported method.[12] Because AEAPMS was used as the main raw material, the obtained CDs carried a large amount of

methoxysilane groups, were highly reactive intermediates responsible for bonding with silanols and hydroxyl groups from the silica-coated $SrAl_2O_4$:Eu,Dy phosphor.

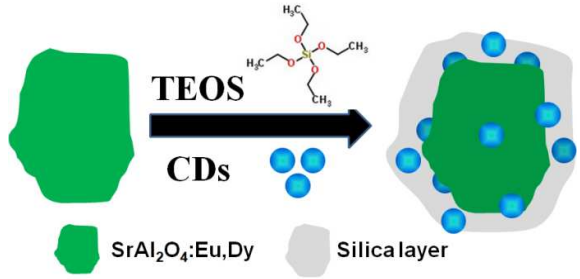

Fig. 1 Schematic illustration of the synthesis procedure of CDs-SAO.

The FT-IR spectra of SAO, CDs, and CDs-SAO are demonstrated in **Fig. 2(a)**. The broad peak at 3485 cm^{-1} corresponds to the O-H stretching vibration. The bands at around 1680 cm^{-1} indicate the existence of carbonyl (C=O) groups. The intensity of -OH groups of the CDs-SAO composite at 3485 cm^{-1} is reduced significantly. Meanwhile, the intensity of Si-O-Si at 1100 cm^{-1} is sharply increased. These data demonstrate that -OH on the surface of SAO enable the formation of silica layer and the possibility of CDs bonding with silanols and hydroxyl groups from the silica-coated SAO. The successfully grafting of the CDs to form CDs-SAO is further confirmed by XPS in **Fig. 2(b)**. The binding energy of O (1s, 532.3 eV); N (1s, 401.3 eV); C (1s, 285.3 eV); Cl (2s, 197.3 eV); and Si (2s, 152.3 eV; 2p, 101.3 eV) can be clearly seen, respectively. However, because XPS is a technique used for surface inspection and its detection depth is less than 10 nm, the absence of the elements belonging to SAO indicates that SAO might be uniformly coated by the silica layer and CDs. From the transmission electron microscopy (TEM) image as shown in **Fig. 2(c)**, we can see that the as-prepared CDs are well dispersed with average sizes of ~10 nm. **Fig. 2(d)** witnessed the transparent surface shell coating of silica layer on the SAO. It can be clearly seen that CDs are conventionally embedded into the silica layer of SAO, suggesting the successfully doping of CDs.

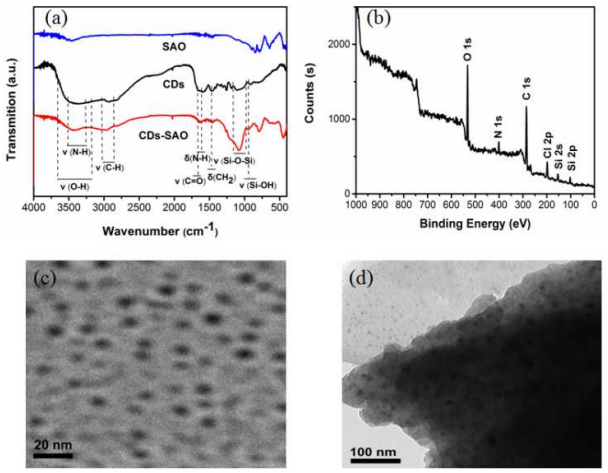

Fig. 2 (a) FTIR spectra of SAO, CDs, CDs-SAO. (b) XPS of CDs-SAO. (c) TEM image of CDs. (d) TEM image of CDs-SAO.

Fluorescence resonance energy transfer (FRET) is practical in its capacity to supply accurate spatial resolution, distant range and sensitivity. FRET involves the excitation energy transferred non-radiatively from an excited donor to a proximal ground-state acceptor.[29] **Fig. 3** shows a general energy level describing dual emission from CDs-SAO, involving two emitters that are coupled closely such that energy transfer (ET) occurs from CDs to SAO. When ET occurs on the same time scale as CDs luminescence, emission is observed from both the CDs and the SAO. As presented in **Fig. 4(a)**, there is a spectral overlap between the excitation of SAO and the emission of CDs, indicating that a slight FRET process from donor (CDs) to acceptor (SAO) might occur. Such an energy transfer behavior has been further confirmed by the lifetime measurements in **Fig. 4(b)**. In order to prove the existence of the ET from the CDs to SAO, the emission decay curves of SAO and CDs-SAO (prepared with a mass ratio of 0.8) are presented, monitored at 520 nm for SAO emission, without and with the sensitizer CDs, respectively. The decay curves are fitted well to a second order exponential Eq. (1):

$$I(t) = I_0 + A_1 \exp(-t / \tau_1) + A_2 \exp(-t / \tau_2) \qquad (1)$$

where, $I(t)$ is the luminescence intensity at time t and I_0 is the background luminescence intensity, A_1 and A_2 are constants, τ_1 and τ_2 are the lifetimes of the exponential components. In addition, the average lifetime constant τ can be calculated using the following Eq. (2):[30]

$$\tau = (A_1\tau_1^2 + A_2\tau_2^2) / (A_1\tau_1 + A_2\tau_2) \qquad (2)$$

the average decay times of SAO and CDs-SAO are calculated to be 5.6 and 10.6 μs, respectively. It is evident that the lifetime for CDs-SAO is larger than that of SAO, the lifetime of SAO acceptor has increased, which confirms the presence of ET from CDs to SAO in present system.

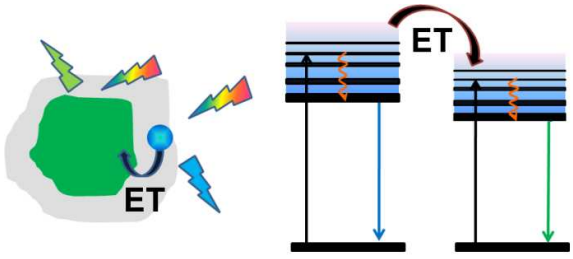

Fig. 3 A general energy level scheme describing dual emission from CDs-SAO composite. Two luminophores interacting through energy transfer (ET).

The Fluorescence spectra of CDs at different excitation wavelength are shown in **Fig. 4(c)**. When excited in the range of 340-380 nm, CDs exhibit strong photoluminescence centered at 450 nm. However, when the excitation wavelength is further increased, the emission of the CDs red-shifts from 450 to 540 nm and the intensity decreased greatly. This is a simple consequence of the lowering of the excitation energy, leaving the various higher emission energy levels inaccessible (adding

on the associated energy for the Stokes shift in each case). The n-π* and the broad surface-state absorption peaks overlap, and the emission energy levels are also fairly broad.[31] Owing to the excitation-dependent photoluminescence emission of CDs, we can easily control the emission wavelength of the donor (CDs) and leads to precise energy matching between the donor and acceptor of the FRET system for more accurate detection.[32] The fluorescence spectra of the CDs, SAO, and CDs-SAO (prepared with a mass ratio of 0.8) are shown in **Fig. 4(d)**. The CDs exhibit blue photoluminescence centered at 456 nm under an excitation wavelength of 370 nm. The SAO generate green emission peaked at 520 nm in the fluorescence spectrum under a 320 nm excitation, attributed to anomalous luminescence originated by Eu^{2+} ions in this host lattice. A dual emission spectrum was displayed at a single excitation wavelength (370 nm), indicating that the CDs-SAO composite was successfully prepared. It is obviously to note that the emission band of CDs in the dual emission spectrum red shifts, due to the high relative content of CDs, this process is likewise driven by consecutive reabsorptions, where each Stokes shift from the previous emission progressively reduces the highest accessible energy level for the next absorption. However, a wide span of energy levels arising from the n-π* and surface-state transitions allows this progressive down shift to continue smoothly over a wide energy range leading to a strong red shift.[31] The synthetic procedure also provides the flexibility to tune the fluorescence emissions. The emission intensities of CDs-SAO with different mass ratio of $SrAl_2O_4$:Eu,Dy phosphor to CDs solution under a 370 nm excitation were shown in **Fig. 5(a)**. With the addition of SAO, the emission spectra at 520 nm appeared and the overall emission intensity increases, owing to the strong green luminescence of SAO.

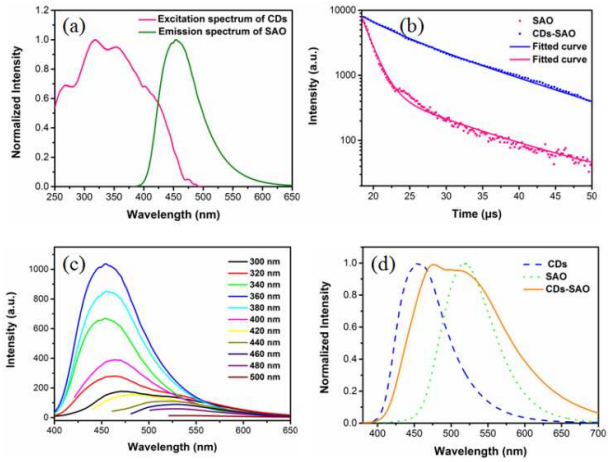

Fig. 4 (a) Excitation spectrum of SAO (monitored at 520 nm) and emission spectrum of CDs (excited at 370 nm). (b) Decay curves of SAO and CDs-SAO monitored at 520 nm excited at 320 nm (prepared with a mass ratio of 0.8). (c) Fluorescence spectra of CDs excited at different excitation wavelength. (d) Fluorescence spectra of CDs (excited at 370 nm), SAO (excited at 320 nm), and CDs-SAO (prepared with a mass ratio of 0.8, excited at 370 nm).

The dual emission spectrum of these hybrid materials provides possibility for temperature sensing. The relative emission intensities result from two closely separated energy levels. When the two energy levels are thermally couple to reach thermal equilibrium, the population of two levels can be depicted by a Boltzmann-type distribution parametrized by temperature. The surrounding temperature can be monitored and measured by using the intensity ratio of the emission from the two thermally couple levels.[33] In addition, the energy separation between the two levels should be small in order for efficient thermal coupling. The ratiometric temperature sensing is expected to be more accurate than single-parameter temperature sensing because it provide self-calibrated results by two readouts.

To evaluate the thermal stability of CDs-SAO (prepared with a mass ratio of 0.8), we conducted TGA in the air atmosphere at a heating rate of 10 °C min^{-1} as shown in **Fig. 5(b)**. The thermogram reveals that CDs-SAO has decomposition point of 263 °C, which demonstrates that CDs-SAO maintains thermal stable in a large temperature range. To apply the potential of CDs-SAO (prepared with a mass ratio of 0.8) as a ratiometric thermometer, the temperature-dependent photoluminescent (PL) properties were investigated under a single excitation wavelength (**Fig. 5(c)**). Owing to the tunable emission properties of CDs under different excitation wavelength, thus a proper excitation wavelength can be selected to display an obvious relative emission characteristic of CDs-SAO. We selected 370 nm as the excitation wavelength of the CDs-SAO under different temperatures. With the increase of temperature from 100 to 400 K, the overall emission intensities substantially decrease due to the thermal quenching effect. Numerous investigations have discussed the thermal quenching behaviours.Two competing factors prevail.[34-35] One is the activation energy of nonradiative relaxation. Excited electrons are promoted to a higher state of vibration excitation energy levels by absorbing external energy at high temperatures. Afterward, these excited electrons relax to the ground state of the activators through a non-radiative manner.[34] And the other is the rate of temperature-induced direct tunnelling, which prevents emissive quenching behaviour of PL. As the temperature increases, the thermally activated luminescent center strongly interacts with the thermally active phonon, the population density of phonon is increased, the electron-phonon interaction is dominant, and consequently the emission spectra are widen.[36] Meanwhile, the peak positions at 520 nm of SAO blueshift with the increasing temperature. To account for the phenomenon, consider that thermally active phonon-assisted tunneling from the excited states of low-energy emission band to the excited states of high-energy emission band in excited states occurs.[37] When temperature increases, the population of 5d electrons at higher-energy sublevel increases due to phonon assisting and thus the emission energy increases, as a result blueshift is observed. The emission intensities at 476 nm of CDs are found red shifts and also decreased with the increasing of the temperature, but the extent of decrease is much less than that of SAO. The exact temperature induced PL quenching mechanism of CDs is still unknown. Several studies have

suggested that it is related to temperature enhanced population of non-radiative channels of surface (trap/defect) states.[38] The emission peak of CDs shifts toward the lower energy mainly due to strong phonon scattering when temperature was increased from 100 to 400 K.[23] The changes in the intensities of the two emission peaks result in fluorescence color changes from yellow to green.

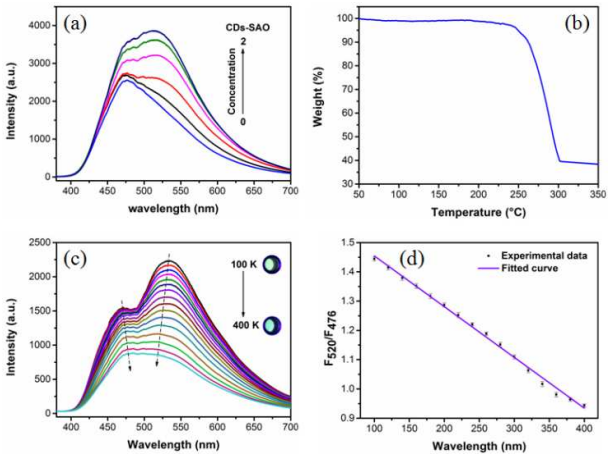

Fig. 5 (a) Fluorescence spectra of CDs-SAO with different mass ratio of SAO to CDs solution: 0, 0.4, 0.8, 1.2, 1.6, 2.0 excited at 370 nm. (b) TGA thermogram of CDs-SAO (prepared with a mass ratio of 0.8). (c) Temperature-dependent emission spectra of CDs-SAO (prepared with a mass ratio of 0.8) recorded every 20 K from 100 to 400 K, excited at 370 nm. Photographs were taken at 100 and 400 K, respectively, under 365 nm UV light (Inset). (d) Temperature-dependent intensity ratio of SAO (520 nm) to CDs (470 nm) and the fitted curve for the composite. The error bars are one standard deviation from the average values collected from the temperature-dependent intensity ratios.

Fig. 5(d) plots the ratio of the two emission intensity at 520 nm (SAO) and 476 nm (CDs) versus temperature, a good linearity was obtained in the range of 100 to 400 K. The linearity can be described as Eq. (3)

$$T = 940.83 - 578.03F_{520} / F_{476} \quad (3)$$

with correlation coefficient 0.996. Where F_{520} and F_{476} are the emission intensity at the monitoring wavelength, respectively, T is the temperature of the CDs-SAO composite system (K). The good linearity indicates that CDs-SAO is an excellent luminescent thermometer operative in the range from 100 K to 400 K. Although several luminescent thermometers have been available, such a linear response throughout the large temperature range has been rarely reported. To further evaluate the reversibility of CDs-SAO as a temperature sensing, cycles were conducted between 100 K and 400 K in Fig. 8(a), display comparatively excellent cycling properties of CDs-SAO, which demonstrate the excellent temperature sensing properties of CDs-SAO in the temperature range from 100-400 K. Once the stress due to higher temperature is relieved by cooling the composite, the trap state population is likely reduced, resulting in recovery of PL intensity.[39] As a rule, the internal sensitivity of any probe can be defined as Eq. (4):[40]

$$S = \frac{\partial(P) / \partial T}{P} \quad (4)$$

where P is the measured temperature-sensitive parameter, such as lifetime, intensity, or intensity ratio. For ratiometric luminescent temperature sensor, the relative sensitivity can be determined as Eq. (5)

$$S = \frac{\partial(I_1 / I_2) / \partial T}{I_1 / I_2} \quad (5)$$

where I_1 and I_2 are the two luminescence intensities of the dual emission.[41] Herein, the sensitivity of CDs-SAO was calculated to be 0.17% K^{-1} .

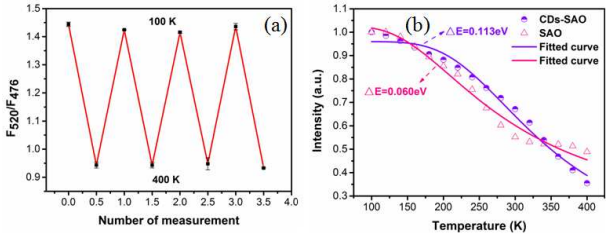

Fig. 6 (a) Temperature-responsive reversibility study of CDs-SAO (prepared with a mass ratio of 0.8) between 100 K and 400 K. The error bars are one standard deviation from the average values collected from the heating-cooling cycling measurements. (b) The integrated emission intensity of SAO and CDs-SAO (prepared with a mass ratio of 0.8) from 100 to 400 K.

Temperature-dependent integrated emission intensity of SAO and CDs-SAO composite in the range of 100-400 K are shown in **Fig. 6(b)**. The integrated emission intensity at 100 K was normalized to 1. The quenching temperature of SAO is about 360 K and quenching temperature of CDs-SAO is about 350 K where the intensity has dropped to half of the intensity at 100 K. According to the classical theory of thermal quenching, the temperature-dependent intensity can be described by the Eq. (6):

$$I(T) = I_0 / [1 + C \exp(-\Delta E / kT)] \quad (6)$$

where I_0 and $I(T)$ are the intensity at temperature T=0 and T(K), respectively. k is Boltzmann's constant while C is a rate constant for the thermally activated escape.[42] ΔE is the activation energy for the thermal quenching process. ΔE of SAO and CDs-SAO are calculated to be 0.060 eV and 0.113 eV, respectively. The lower value of ΔE means a more rapid nonradiative rate at a given temperature. Thus, compared with the SAO, the thermal stability of CDs-SAO is enhanced. It indicates that CDs-SAO could be used as potential candidates for optical temperature sensors in terms of the thermal stability.

4 Conclusions

In summary, the carbon dots (CDs) grafted $SrAl_2O_4$:Eu,Dy phosphor composite (CDs-SAO) as a ratiometric temperature sensor was prepared via a facile one-step sol-gel method. The

formation of a silica layer on the surface of $SrAl_2O_4$:Eu, Dy phosphor (SAO) enables CDs to be coupled on the layer through the silylation reaction at the same time. A dual emission spectra are displayed at a single excitation wavelength (370 nm), indicating that CDs-SAO was successfully prepared. Because SAO emission is highly temperature dependent while CDs emission is less sensitive to temperature, we used the CDs emission as an internal reference to construct a ratiometric temperature sensor. The as-prepared composite has a wide linear temperature sensing range that matches well with the physiologically relevant temperatures. The CDs-SAO exhibits tunable emission and has been proved to be an ideal candidate as a ratiometric temperature sensor in this work, providing the economical and accessible approach for measuring local temperature in even complex conditions.

Acknowledgements

The present work was supported by the National Natural Science Foundations of China (Grant Nos. 51203053, 51372091), the Teamwork Projects funded by the Guangdong Natural Science Foundation (Grant No. S2013030012842) and the Key Academic Program of the 3rd phase '211 Project' of South China Agricultural University.

Notes and references

1 C. D. Brites, P. P. Lima, N. J. Silva, A. Millán, V. S. Amaral, F. Palacio and L. D. Carlos, *Nanoscale.,* 2013, **16**, 7572.
2 Z. Boruc, M. Kaczkan, B. Fetlinski, S. Turczynski and M. Malinowski, *Opt. Lett.,* 2012, **24**, 5214.
3 L. Lu, G. Yang and Y. Xia, *Anal. Chem.,* 2014, **13**, 6188.
4 X. Wang, O.S. Wolfbeis and R. J. Meier, *Chem. Soc. Rev.,* 2013, **19**, 7834.
5 E. J. McLaurin, L. R. Bradshaw and D. R. Gamelin, *Chem. Mater.,* 2013, **8**, 1283.
6 K. Okabe, N. Inada, C. Gota, Y. Harada, T. Funatsu and S. Uchiyama, *Nat. Comm.,* 2012, **3**, 705.
7 T. Tsuji, S. Yoshida, A. Yoshida and S. Uchiyama, *Anal. Chem.,* 2013, **20,** 9815.
8 H. Hu, L. Xiong, J. Zhou, F. Li, T. Cao and C. Huang, *Chem-Eur J.,* 2009, **14**, 3577.
9 J. Lee and N. A. Kotov, *Nano Today.,* 2007, **1**, 48.
10 H. Peng, M. I. Stich, J. Yu, L. Sun, L. H. Fischer and O.S. Wolfbeis, *Adv. Mate.,* 2010, **6,** 716.
11 X. Chen, Q. Jin, L. Wu, C. Tung and X. Tang, *Angew Chem., Int, Ed.,* 2014, **46**, 12542.
12 F. Wang, Z. Xie, H. Zhang, C. Liu and Y. Zhang, *Adv Funct Mater.,* 2011, **6**, 1027.
13 F. Wang, S. Pang, L. Wang, Q. Li, M. Kreiter and Y. Liu, *Chem Mater*, 2010, **22**, 4528.
14 X. Li, M. Rui, J. Song, Z. Shen, and H, Zeng, *Adv. Funct. Mater.,* 2015, **25**, 4929.
15 D. Jaque and F. Vetrone, *Nanoscale*, 2012, **4** , 4301.
16 G. W. Walker, V. C. Sundar, C. M. Rudzinski, A. W. Wun, M.G. Bawendi and D. G. Nocera, *Appl. Phys. Lett.,* 2003, **83**, 3555.
17 N. Chandrasekharan and L. A. Kelly, *J. Am. Chem. Soc.,* 2001, **123** , 9898.
18 X. Li, Y. Liu, X. Song, H. Wang, H. Gu and H. Zeng, *Angew. Chem. Int. Ed.,* 2015, **54**, 1759.
19 M. Sun, S. Qu, Z. Hao, Ji, P. Jing, H. Zhang, L. Zhang, J. Zhao and D. Shen, *Nanoscale*, 2014, **6**, 13076.
20 I.U. Arachchige and S.L. Brock, *J. Am. Chem. Soc.,* 2007, **7** 1840.
21 B. C. Satishkumar, S. K. Doorn, G. A. Baker and A. M. Dattelbaum, *ACS Nano.,* 2008, **11**, 2283.
22 H. Tetsuka, T. Ebina and F. Mizukami, *Adv. Mater.,* 2008, **16**, 3039.
23 S. A. Wade, S. F. Collins and G. W. Baxter, *J. Appl. Physic.,* 2003, **8**, 4743.
24 V. K. Rai, *Appl. Phys. B*, 2007, **88**, 297.
25 A. Pandey and V. K. Rai, *Appl. Phys. B*, 2013, **113**, 221.
26 G. Tripathi, V. K. Rai and S. B. Rai, *Appl. Phys. B*, 2006, **84** 459.
27 X. Lü, *Mater. Chem. Phys.,* 2005, **93**, 526.
28 J. Zhang and J. R. Lakowicz, *Opt. Express,* 2007, **5**, 2598.
29 R. Mi, C. Zhao and Z. Xia, *J. Am. Ceram. Soc.,* 2014, **6**, 1802.
30 C. Yu, X. Li, F. Zeng, F. Zheng and S. Wu, *Chem. Comm.* 2013, **4**, 403.
31 Y. Wang, S. Kalytchuk, Y. Zhang, H. Shi, S. V. Kershaw and A. L. Rogach, *J. Physic. Chem. Lett.,* 2014, **8**, 1412.
32 V. Chernov, T.M. Piters, R. Meléndrez, W.M. Yen, E. Cruz-Zaragoza and M. Barboza-Flores, *Radiat. Meas.,* 2007, **4**, 668.
33 C. Lin and R. Liu, *J. Solid State Light.,* 2014, **1**, 1.
34 J. Kim, A. Kwon, Y. Park, J. Choi, H. Park, G. Kim, *J. Lumin.,* 2007, **583**, 122.
35 C. Lin, Z. Xiao, G. Guo, T. Chan and R. Liu, *J. Am.Chem. Soc.*, 2008, **43**, 5658.
36 J. Kim, Y. Park, G. Kim, J. Choi, H. Park, *Solid State Commun.,* 2005, **133**, 445.
37 D. Valerini, A. Creti, M. Lomascolo, L. Manna, R. Cingolani and M. Anni, *Phys. Rev. B,* 2005, **23**, 235409.
38 G. Eda, Y. Lin, C. Mattevi, H. Yamaguchi, H. Chen, I. Chen, C. Chen and M. Chhowalla, *Adv. Mater.,* 2010, **22**, 505.
39 V. Biju, Y. Makita, A. Sonoda, H. Yokoyama, Y. Baba and M. Ishkawa, *J. Phys. Chem. B*, 2005, **109**, 13899.
40 A. E. Albers, E. M. Chan, P. M. McBride, C. M. Ajo-Franklin, B. E. Cohen and B. A. Helms, *J. Am. Chem. Soc.,* 2012, **23**, 9565.
41 A. Cadiau, C. D. Brites, P. M. Costa, R. A. Ferreira, J. Rocha and L.D. Carlos, *ACS Nano.,* 2013, **8**, 7213.
42 V. Bachmann, C. Ronda, O. Oeckler, W. Schnick and A. Meijerink, *Chem. Mater.,* 2008, **2**, 316.